No. 558 January 2017

Reactive Flow Simulation of Micromixers Based On Grid Deformation Techniques

O. Mierka, M. Munir, C. Spille,
J. Timmermann, M. Schlüter, S. Turek

ISSN: 2190-1767

Reactive Flow Simulation of Micromixers Based On Grid Deformation Techniques

Otto Mierka[a,*], Maimoona Munir[a], Claas Spille[b], Jens Timmermann[b], Michael Schlüter[b], Stefan Turek[a]

Abstract

Process intensification of engineering applications in the framework of reacting flows in micromixer devices attracts the attention of engineers and scientists from various fields. With the steadily increasing available computational resources the traditional experimentally supported investigations may be extended by computational ones. For this purpose, a simulation framework based on state of the art numerical techniques extended with special grid deformation techniques has been developed. Its validation in terms of comparison with computational and experimental results in reacting, as well as in non-reacting frameworks has been performed on the basis of the T-mixer, and SuperFocus mixer, respectively. The computational efficiency of the developed tool is shown to be applicable for optimization tasks, such as reverse engineering purposes.

Keywords

grid deformation, reactive liquid flow, one-way coupling, stationary simulation, micromixers

Introduction

Interdigital micromixers provide a novel technology that allows to accomplish a nearly complete homogenization of two or more segregated fluid streams within short contact times in relation to the time for a fast chemical reaction. They are also used for reactions, extractions, liquid-liquid dispersions, measurements of dispersion, measurements of diffusivities and determination of kinetic rate constants. There are many aspects in which specific research and development is required as for biologists, chemists or chemical engineers with the aim to make them suitable for industrial purposes. During the design of micromixers the estimation of mixing performance is associated with a given lamellar thickness, expected concentration gradients and orientation of intermaterial surfaces in relation to the arising deformation tensor (Malecha *et al*. [1]). Cerbelli and Giona [2] discussed the analytical techniques and assumptions on the interdigital micromixers. Panic *et al.* [3] developed experimental approaches to investigate the mixing performance and verified on different micromixers (based on mixing principle and geometry). Thanks to the use of glass micromixers Hessel *et al.* [4] and Löb *et al.* [5] increased the knowledge regarding chemical processing in interdigital micromixers. With development of glass mixers in 2000 the door to hydrodynamic information for micromixing devices was practically unlocked and Hoffmann et al. provided first insights into three-dimensional concentration fields for reactive flows in glass covered silicon T-mixers [6]. The pioneering work of Hardt and Schönfeld [7] pushed further the

[a] Dortmund University of Technology, Faculty of Mathematics, Chair of Applied Mathematics and Numerics, Vogelpothsweg 87, 44227, Dortmund, Germany. [b] Hamburg University of Technology, Institute of Multiphase Flows, Eissendorfer Str. 38, 21073 Hamburg, Germany.
[*] Corresponding author: otto.mierka@mathematik.tu-dortmund.de

boundaries of knowledge by comparing and optimizing the interdigital micromixers by CFD analysis and suggested the focusing of many inlet streams to a narrow mixing channel. The SuperFocus and slit-shaped mixer were found to be superior to the triangular and rectangular mixer, in terms of mixing times with respect to the mixing length scales. The mixing time is in the range of milliseconds providing favorable, well-defined process conditions for fast chemical reactions, and the decrease of residence time by geometric focusing.

Numerical simulations in the framework of micromixer applications are expected to contribute to the understanding and to the optimization of the underlying phenomena so to help to their implementation in industrial processes. However, the use of numerical techniques in a form of black-box simulation tools is not as straightforward, since the resolution of the employed discretization schemes plays a crucial role in determining their suitability for the given applications. From the hydrodynamics point of view the processes occurring in micromixers are mostly convection dominated and therefore they require the use of appropriate numerical schemes being able to suppress numerical diffusion as much as possible. Studies for appropriate numerical schemes to tackle certain micromixer applications were reported, such as the 'split and recombine' (Glatzel *et al.* [8]) or the T-mixer (Bothe *et al.* [9]) or even in the framework of interdigital mixers (Hessel *et al.* [5]). In the current work we extend the state of the art numerical techniques with an additional grid deformation technique which contributes to the overall numerical scheme by gaining additional resolution which is achieved by concentrating the mesh elements in the regions characterized by high values of gradients of the transported scalar quantities. The complete numerical scheme is realized in the framework of finite elements (Q_1) in the parallel 3D version of the open-source software package FeatFlow. Besides of the grid deformation method, there are the following numerical techniques being incorporated:

- Algebraic Flux Correction (AFC) which is by construction designed to be a non-linear stabilization scheme guaranteeing a positivity-preserving high resolution transport of scalar quantities. The algebraic realization of the particular AFC method follows the work of Kuzmin *et al.* [10].
- Operator Splitting (OS) technique of scalar transport equations is used in order to split the different time scales of transport in physical coordinates (convection, diffusion) from the transport in the species dimension (reaction).
- Projection based interpolation methods which allow the parallel usage of different types of meshes being appropriate for the different transport problems. This method allows the strategy of performing flow simulations on relatively coarse and unstructured (not deformed) meshes and the obtained flow fields are dynamically interpolated onto the highly deformed meshes used for the scalar transport equations.

The use of these numerical techniques exploits a synergic effect and guarantees high computational efficiency in terms of delivering the most accurate predictions for the given price of computational times which promotes them to be used in optimization frameworks.

Algebraic Grid Deformation Technique (AGD)

Local increasement of resolution in computational schemes is a very advantageous procedure because it may extend the accuracy of a given CFD simulation tool by several orders. Strictly speaking, there are three fundamentally different numerical techniques being available known as *h*-, *r*- and *p*- adaptivity, which are theoretically possible to further combine with each other. Our focus is related to the so called *r*-adaptivity which has the advantage of using static structures, only

the coordinates of the given topological mesh are changed and concentrated according to the embedded monitor function. For this reason an additional mechanism is needed to be included into the numerical scheme called as the Arbitrary Lagrangian Eulerian method which accounts for the additionally arising mesh velocity reflecting the movement of the mesh coordinates. The deformation of the mesh points according to state of the art numerical techniques standing on solid mathematical grounds (see Cai *et al.* [11], Grajewski [12] or Paul [13]) is performed on the basis of the solution of a nonlinear diffusion based PDE system to steady state, the realization of which in every time step is a rather time expensive operation, decreasing the practical appeal of the underlying method. Before addressing the detailed description of the AGD technique developed for the simulation of transport equations exhibiting steep gradients we would like to point out that up to our knowledge such a realization was not reported before and its ability is not constrained only for such scalar transport simulations but also in the framework of other engineering applications involving moving boundaries, or flows influenced by shear dependent rheological models. The first important attribute making our approach different from others described in the literature is that the realization is only algebraic and not PDE based. However, as it is also realized in typical PDE based GD techniques, the core of our technique is related to a construction of the so-called monitor function $M(\mathbf{x})$, being responsible for addressing the required size distribution of the resulting mesh elements while sustaining their original and therefore constant topology. The carefully constructed monitor function is then transformed into a weight distribution $w(\mathbf{x})$ within an iterative (repetitive) algebraic mesh smoothening procedure, also known as 'Laplacian' smoothening with the difference that these procedures have been so far preferred only to correct or smooth the deformed mesh predicted by classical PDE based techniques, which corresponds to an isotropic setting of the weight distribution $w(\mathbf{x}) > 1$. According to our realization, the time-expensive PDE prediction step can be completely skipped and equivalently substituted with an anisotropic counterpart of the Laplacian mesh smoother operating by means of a corresponding weight distribution $w_j(\mathbf{x})$as follows:

$$\mathbf{x}_i^{\text{new}} = (1-\omega).\mathbf{x}_i^{\text{old}} + \omega \frac{\sum_{j=1,N_\text{V}}^{if\ \exists\ e_{ij}} w_j \mathbf{x}_j^{\text{old}}}{\sum_{j=1,N_\text{V}}^{if\ \exists\ e_{ij}} w_j} \quad \text{for} \quad i = 1,\dots,N_\text{V} \tag{1}$$

Here $\mathbf{x}$ are the mesh vertex coordinates, e_{ij} are the edges connecting the element vertices, ω is the underrelaxation parameter (usually set to 0.25), and N_V is the total number of mesh nodes. The only drawback, stemming from a strictly mathematical point of view is that we cannot guarantee or prove (yet) the properties of the generated deformed mesh, but as experienced on the number of processed examples [14, 15] we observe the robustness of the proposed numerical technique. The construction of the monitor function $M(\mathbf{x})$ is in fact arbitrary, it may reflect or combine different aims expected from the deformation since it can react on field data such as gradient (concentration, temperature, velocity) distributions or a signed distance function $d(\mathbf{x})$ representing the distance distribution to the closest interface. Our choice in the framework of transport equations exhibiting steep gradients is based on the first option, since this may help to adapt the mesh especially in the regions characterized by high values of derivatives which will be more accurately resolved on the highly adapted meshes. The recovered gradient distributions of the chemical species are then used to be converted into a global Monitor function $M(\mathbf{x})$ addressed by only one single field. This conversion is achieved by taking the maximum of all available gradient fields,

so to allow the mesh deformation algorithm to adapt simultaneously to local fine structure features referring to the different chemical species. According to the current realization of the grid deformation method there are no run-time grid-quality monitoring/correction mechanisms introduced, instead, the strategy of built-in threshold is to be applied within the designed monitor function. In light of the below presented numerical examples the particular construction of $M(\mathbf{x})$ is given as follows:

$$M(\mathbf{x}) = \max_{i=1,\dots N_S} \left(M_0, M_0 + \log(\|\nabla c(\mathbf{x})_i\|)\right)^{M_1} \tag{2}$$

In (2) M_0 defines the lower threshold value, M_1 defines the extent of the deformation, and i are the chemical species present in the system. Both parameters, M_0 and M_1, depend on the particular application, meaning that their values are subjected to adjustment w.r.t. the required mesh resolution and simulation convergence criterions.

Description of the Complete Computational Framework

The focus of the proposed computational framework is designed for application in the field of micromixer simulations where the encountered flow regimes are prevailingly steady. This fact defines the applied solution strategy, which is as follows:

1. Compute the stationary velocity field for the given flow rate and fluid properties,
2. Interpolate the velocity solution to the deformed scalar transport computational grid,
3. Simulate the scalar transport of species in an operator splitting fashion towards steady state,
4. Deform the computational grid according to the recovered gradients and the resulting monitor function,

Where the first step needs to be performed only once and the steps 2 to 4 are iterated over until steady state (no further movement of the computational grid) is reached. For the fluid dynamics simulations, in general, relatively coarse meshes are to be used, since the velocity distributions do not experience such strong gradients as the concentration of the species being transported on the underlying velocity solutions. Another numerical ingredient greatly accelerating the steady state solution of the resulting system is related to the employed geometric multigrid structures which allow a cheap ‘prediction’ on a one level coarser resolution, the result of which is being prolonged as an initial guess to the fine level resolution ‘correction’ step. The last special numerical ingredient needed to be mentioned is the solution transfer from one computational mesh to another one. Since, the solution of the steady velocity field is performed on a lightly unstructured but not deformed computational mesh, it needs to be interpolated several times to the highly distorted computational mesh used for the scalar transport problem. In this case, exploiting the high order approximation of the underlying FEM technique an L_2 projection is utilized, according to which all integration point coordinates from the deformed mesh are collected (eventually communicated due to the parallel framework) into which the corresponding velocity is interpolated.

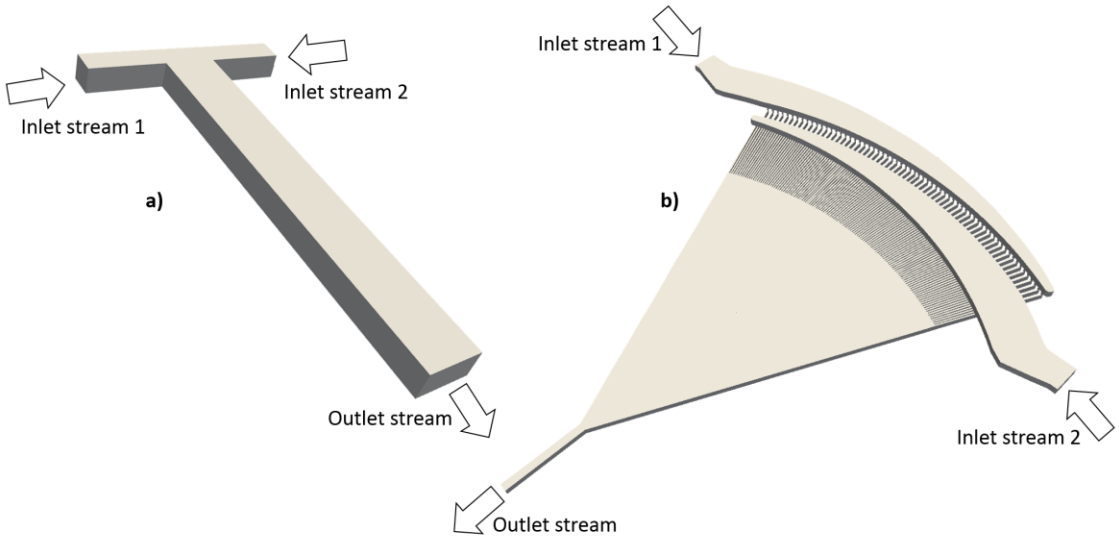

Fig 1 Computational domains used for the a) T-micromixer and for the b) SuperFocus Mixer simulations.

Validation of the Simulation Framework

In this section the validation of the developed reaction module on the so called T-mixer problem is presented, which is very well suitable for validation purposes since it is supported not only by experimental but also by computational results. The problem deals with a laminar flow according to which the two equal flowrate streams containing the different reactants are introduced into the T shaped mixer (see Fig. 1a) which for the given Reynolds number results in different flow regimes. Following the proposed parameter setup from Bothe et. al [9] three different Reynolds numbers (*Re*=120 segregated flow, *Re*=146 onset of the engulfment flow, and *Re*=186 engulfment flow) have been taken into account. The such chosen range of Reynolds numbers guarantees a stationary operation of the micromixer and hence allowing us to apply the one-way coupled simulation framework described in the previous chapter. One has to note that a considerably pronounced mixing efficiency may be achieved by an unsteady asymmetric (higher *Re*) operation of the micromixer. In the system described above the following neutralization reaction

$$\mathrm{Na\,OH} + \mathrm{H\,Cl} \rightarrow \mathrm{Na\,Cl} + \mathrm{H_2O} \tag{3}$$

was considered to take place. The Schmidt number of the corresponding chemical species was assumed to be on the order of 300, which directly suggests the occurrence of steep gradients being present in the mixing channel. Since the underlying chemical reaction is nearly instantaneous ($k_{\mathrm{CR1}} = 10^{11} L\, mol^{-1} s^{-1}$) the transformation introduced by Toor and Chiang [16] was adopted according to which the transport of one single concentration field only, $\phi := c_{\mathrm{OH^-}} - c_{\mathrm{H^+}}$, needs to be simulated. The physical interpretation of this quantity ϕ is that where it is positive, it represents the concentration of $\mathrm{OH^-}$ ions and where it is negative, it represents the negative concentration of the $\mathrm{H^+}$ ions, since the coexistence of $\mathrm{OH^-}$ and $\mathrm{H^+}$ ions is not possible due to the undergoing instantaneous chemical reaction. As shown by Bothe [4], the introduced concentration transformation may be extended to different molecular diffusivities of the underlying species, as

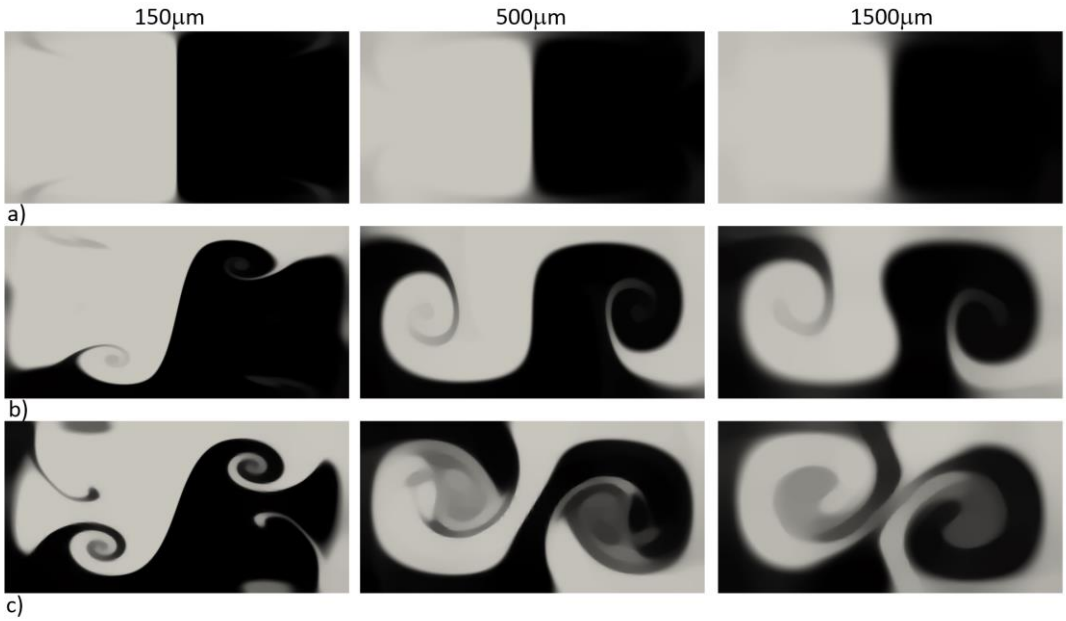

Fig 2 Simulation results for the T-micromixer at different downstream positions in the mixing chamber for different flow regimes characterized by the Reynolds number a) $Re = 120$, b) $Re = 146$, c) $Re = 186$.

well. Here instead, for simplicity reasons, their values has been considered to be identical. Since the flow is dominated by convection, steep gradients of concentrations arise, for which proper numerical treatment is inevitable to determine the conversion of the chemical reaction, which was not the aim of our validation, but can be achieved by corresponding postprocessing of the obtained computational result. Instead, here the aim is to show the robustness of the incorporated numerical ingredients which provide numerical results for nearly similar computational costs associated to the same number of elements ($N_{\mathrm{EL}} \cong 10^6$) as in the original reference but extends the resolution of the underlying numerical framework as displayed in Fig 2. The figure compiles the distribution of the quantity ϕ at different cutplanes for the three different flow regimes. As it may be seen at the cutplanes, the presence of sharp concentration gradients is observed to occur especially in regions characterized by high fluid velocities, while a bit more diffused transition is predicted in regions located in the vicinity of the walls characterized by lower velocities. In addition a gradual smearing can be observed in the axial direction downstream of the mixing channel. For comparison with the corresponding computational and experimental results, the reader is referred to [9]. The deformation of the computational mesh for the different flow regimes at a cutplane 0.5mm downstream in the mixing channel is demonstrated in Fig 3, which is highly concentrated in the regions covering the high gradients of the transported scalar quantity ϕ and coarser at locations where the distribution of ϕ is smooth.

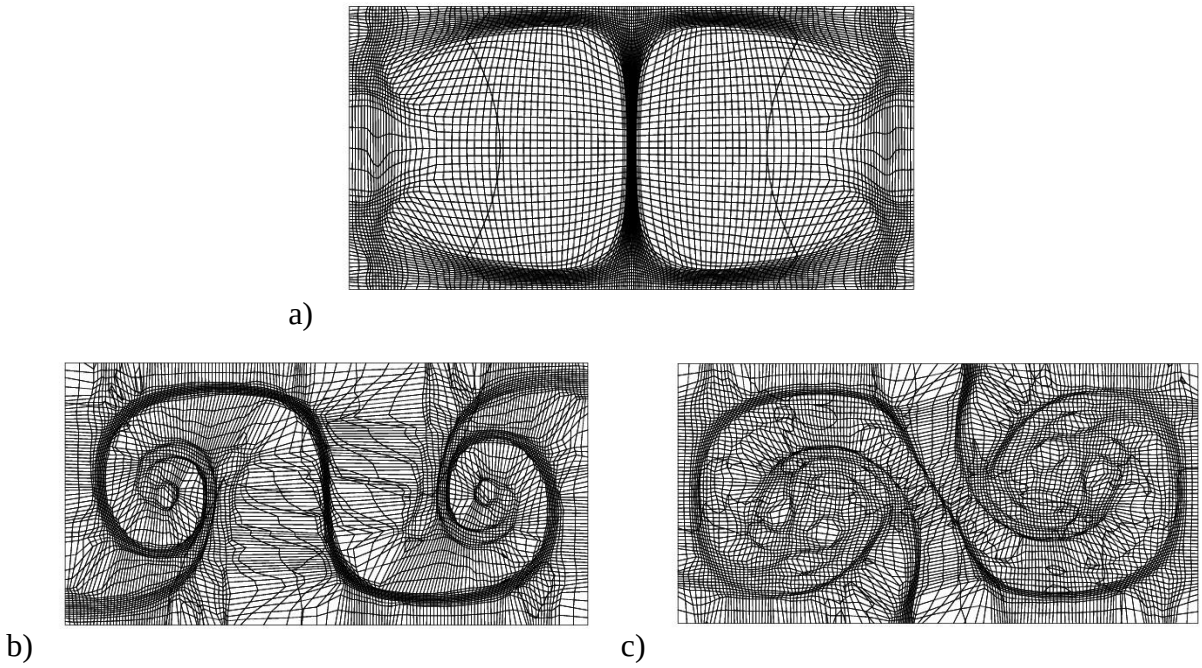

Fig 3 Visualization of the computational mesh for the T-micromixer simulations associated with the different Reynolds numbers a) $Re = 120$, b) $Re = 146$, c) $Re = 186$.

SuperFocus Micromixer - Experimental Setup

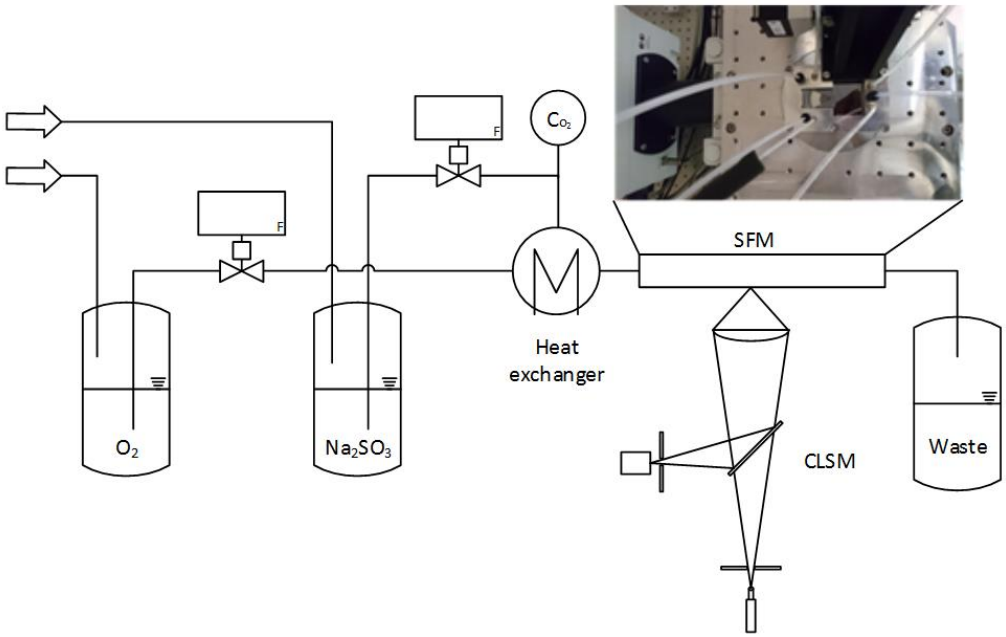

Fig 4 Schematic setup of the sodium sulfite oxidation measurement.

The experimental investigation of local concentration fields for physical and reactive mixing within the SuperFocus mixer (SFM) takes place at the Institute of Multiphase Flows of the Hamburg University of Technology. For the visualization of these concentration fields a confocal laser scanning microscope (CLSM, Olympus FluoView 1000) in combination with a needle-type oxygen micro sensor (PreSens Microx TX-3) is used. A scheme of the experimental setup is shown in Fig 4. The measurement principle is based on an energy transfer due to collision of dissolved triplet oxygen molecules with excited dye species. The collision leads to a deactivation of the physical excitation. Moreover, the decrease of the emitted fluorescence and henceforth the oxygen consumption due to chemical reactions can be optically detected. For all measurements an aqueous solution of $0.03\ g\ L^{-1}$ ruthenium complex Dichlorotris (1, 10-phenanthroline) ruthenium (II) hydrate is prepared. In case of catalyzed reactions, cobalt sulfate hydrate ($0.016\ g\ L^{-1}$) is additionally added. This dye solution is divided into equal shares, one part of the solution is saturated with atmospheric oxygen and the other part is saturated with nitrogen to desorb all oxygen. Afterwards Sodium Sulfite is added to the nitrogen saturated solution and the solution is homogenized manually by shaking. Both streams are poured by a conveying pressure of $0.5\ bar$. The flowrates for three different cases are set and controlled by two Coriolis Mass Flow Meters (mini Cori-Flow M13, Bronkhorst®): $150\ cm^3\ h^{-1}$, $75\ cm^3\ h^{-1}$ and $15\ cm^3\ h^{-1}$, per stream. Before each experiment, the stated fluorescence intensity values are calibrated by using the prepared dye solution with different oxygen concentrations. In the stationary state, every intensity value (gray value) can be dedicated to a certain oxygen concentration by means of the oxygen sensor. Henceforth evaluation based on Stern-Volmer delivers the dependence of the fluorescence intensity to the concentration of oxygen. The SFM could be positioned with an X-Y table in horizontal and vertical direction. Thereby, nine different positions are recorded in high resolution 2D and 3D. The temperature is set and controlled by an air conditioned box around the CLSM and additionally by a cooling zone implemented within the SFM. Supplementary the inflows are temperature controlled through a heat exchanger positioned in front of the SFM inlets. These systems ensure a constant temperature of $20℃ \pm 0.5℃$ in each measurement.

SuperFocus Micromixer - Simulation Results

In this section the simulation results achieved for the SuperFocus mixer (SFM) will be described. The simulations were performed in two subsequent stages, first in a non-reactive framework and subsequently in a reactive framework. The chosen simulation strategy allows the validation of the flow field predicted by the CFD simulation so to reduce the number of possible sources of inconsistencies between simulation and experiment.

From the point of view of simulations the geometry of the SFM consists of three different parts (see Fig 1b)

1) the distributor, being responsible for equally distributing the flowrate of the inlet streams into the mixing chamber,
2) the tapering shape mixing chamber itself
3) and the residence channel directing the interdigitally mixed fluid away from the mixing chamber

Depending on the simulation framework different parts of the complete geometry were taken into account. For the flow simulations all three parts were considered so to account for a realistic

uneven inflow distribution of the streams, and a realistic outflow profile of the fluid leaving the mixing chamber. On the other hand, the subsequent scalar transport simulations were performed only in the tapering shaped geometry of the mixing chamber, since a) upstream the inflow positions the streams exhibit a pure composition being identical to the feed streams entering the SFM unit and b) further mixing in the residence channel was not in focus of the investigations.
According to the first setup referring to the physical mixing framework a flowrate of the inlet streams was set to the highest ($150\ ml\ h^{-1}$+$150\ ml\ h^{-1}$) so to adjust the necessary mesh resolution for the configuration referring to the limit case in terms of the expected occurrence of the steep gradients in the solution. Since other cases characterized by either smaller flowrates or occurrence of chemical reactions will naturally lead to concentration distributions exhibiting smoother transitions as in the most limiting case described above. The experimentally measured value of diffusion coefficient of O_2 in water is $D_{O_2/H_2O} = 2.0\ 10^{-9}\ m^2\ s^{-1}$ which was used as an input parameter into the corresponding scalar transport simulations. The physical parameters of the fluid correspond to the properties of water saturated with air ($\rho = 1000\ kg\ m^{-3}$, $\mu = 10^{-3} Pa\ s$).

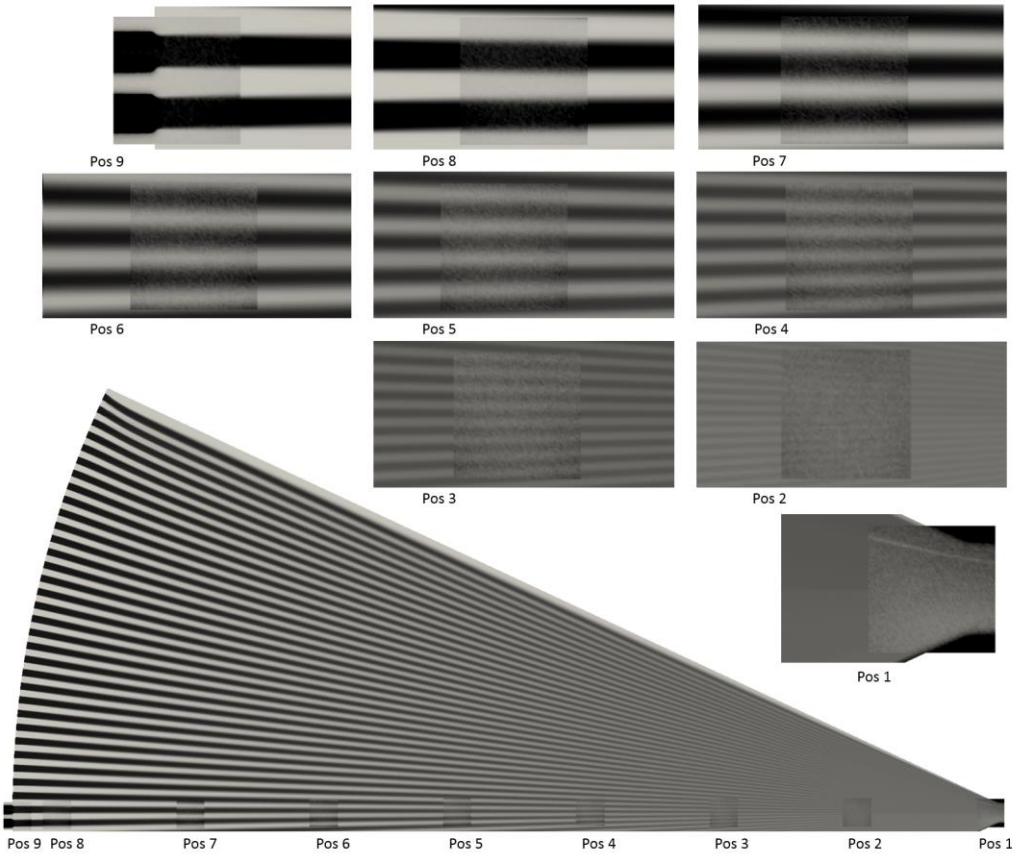

Fig 5 Simulation results obtained for the SuperFocus mixer for physical mixing of O_2 at different axial positions (0.0, 6.0, 9.0, 12.0, 15.0, 18.0, 21.0 and 22.0 mm away from the outflow from the SFM) in the middle cut-plane of the geometry (depth is 0.25 mm). The greyscale corresponds to 0 to 10.5 $mg\ L^{-1}$.

Concerning the most important geometrical parameters as the length, inlet width, outlet width and depth of the SFM (designed and fabricated by the Institute of Micro System Technology, Hamburg University of Technology; based on the design of Invenios) are as follows: $22.0\ mm, 19.84\ mm, 0.5 mm, 0.5\ mm$ with the underlying contraction angle of $50°$. The number of inflow streams is 2×64 with a cross-section of $0.1mm \times 0.5mm$ and width of the separating walls between them is $0.06\ mm$. The experimental sampling locations detecting the luminescence of the quencher were defined at the symmetry axis locations $0.0, 3.0, 6.0, 9.0, 12.0, 15.0, 18.0$ and $21.0\ mm$ upstream from the outlet from the mixing chamber of the SFM. The positions are numbered as $1,2, \ldots 8$ and the ninth position covering the inflow region. The size of the windows at the given position is of $0.64\ mm\times0.64\ mm$ size in the middle cross-section (with respect to depth), unless stated otherwise. In order to provide a comprehensive insight into the comparison between the computational and experimental results, displayed in Fig 5, the experimentally measured pictures were rendered into the environment of the corresponding computational results. Even though, small differences are visible between the results at the given locations, the change of the intensity of the signal at different locations provides an excellent correlation between the experimental and computational results.

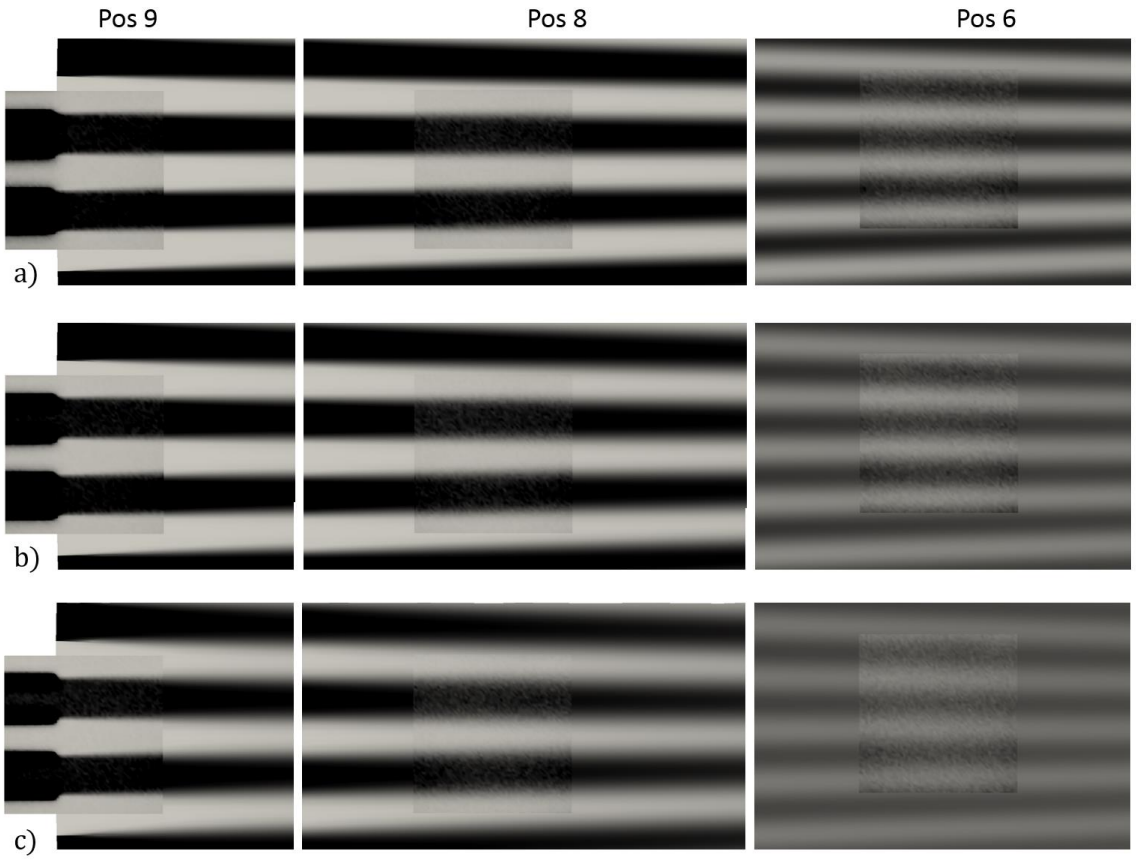

Fig 6 Simulation results obtained for the SuperFocus mixer for physical mixing of O_2 at different axial positions ($18.0, 21.0$ and $22.0\ mm$ away from the outflow from the SFM) at the following depths: a) $0.15\ mm$, b) $0.08\ mm$, c) $0.02\ mm$. The greyscale corresponds to 0 to $10.5\ mg\ L^{-1}$.

The interplay between diffusion and convection resulting in a gradual smearing of the signal in the circumferential direction is also observed to be in a very satisfactory agreement, which justifies the model and its prediction ability. Exploiting the possibilities of the experimental setup snapshots of the O_2 concentration profiles have been measured at different depths at the inflow region (Position 7,8 and 9) which have been compared with the distributions being computationally predicted at the corresponding locations. This comparison is displayed in Fig. 6, which clearly shows the development of the concentration front towards the base-wall of the SFM, where the diffusion mechanisms are more pronounced leading to a more intensive diffusion of O_2 and its penetration into the neighboring inert streams. The demonstrated simulation results were achieved on a sequence of two resolution meshes corresponding to $N_{EL} = 0.8\,10^6$ and $N_{EL} = 6.4\,10^6$ elements which guarantee mesh independence of the obtained computational results. The related computational time on a 16 core Intel Xeon compute server were for the fine level computations on the order of 4-5 hours, which in case of use of a circumferentially equally distributed mesh providing the same resolution in the concentration front region would be incomparably higher leading to practical limitations of computational analysis. The corresponding deformations of the mesh providing such investigations are demonstrated in Fig. 7 which shows the mesh at the symmetry cutplane at different radial positions from the inlet towards the outlet of the SFM. From the mentioned pictures is visible how the mesh is adapted at the high concentration gradient locations and how this adaptation is gradually being relaxed with the extent of smearing of the concentration signal due to the presence of physical diffusion.

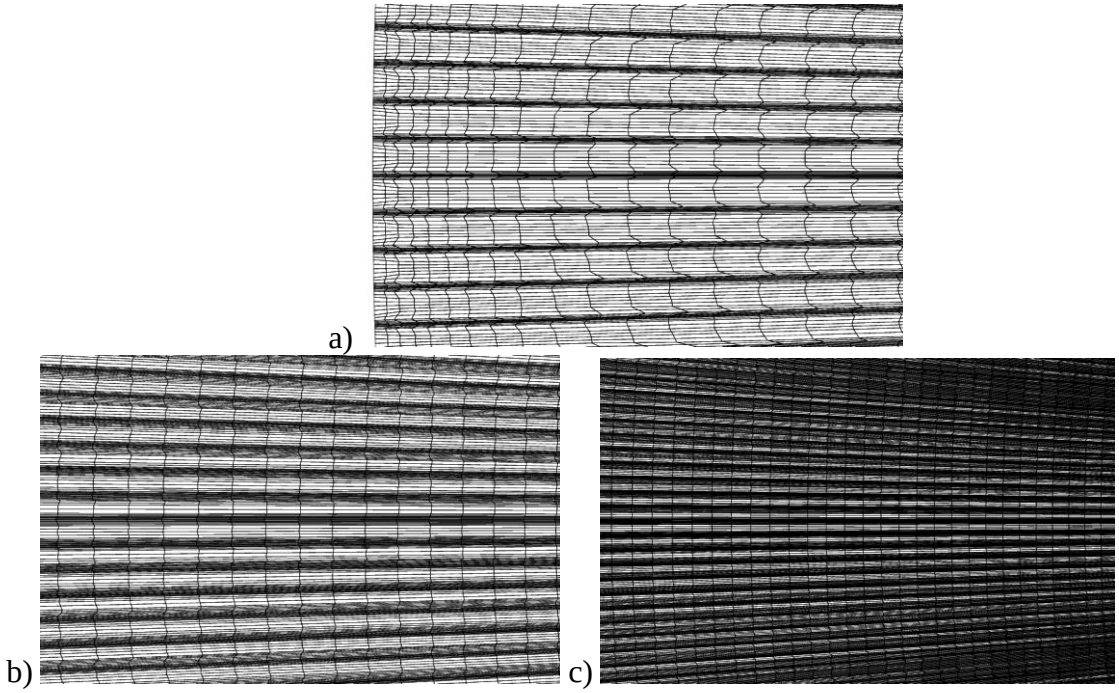

Fig 7 Visualization of the deformed computational mesh used for the physical mixing simulations at different positions in the middle cut-plane (depth is $0.25\ mm$).

In the next stage the simulations were performed in the reactive framework to follow the corresponding measurements of O_2 concentration being affected by the additional chemical reaction:

$$2SO_3{}^{2-} + O_2 \rightarrow 2SO_4{}^{2-} \quad (4)$$

This reaction is not fast by itself therefore it has been catalyzed by cobalt sulfate hydrate which was homogeneously mixed into both inlet streams, therefore its additional simulation could be avoided. Nevertheless, the catalyzer has an influence on the reaction rate constant k_{CR2} which relates the rate of consumption of O_2, according to a bimolecular reaction mechanism, as follows:

$$k_{O_2} = \frac{d\, c_{O_2}}{dt} = k_{\mathrm{CR2}}\, c_{SO_3{}^{2-}}\, c_{O_2} \quad (5)$$

The concentration of the solved O_2 in the first inlet stream was kept at the saturation level of air ($\sim 0.012\ g\ L^{-1}$, corresponding to the given pressure level) and the concentration of the Sodium Sulfite in the second inlet stream was adjusted to $0.4\ g\ L^{-1}$, which results in a roughly 10 times excess of the Sulfite with respect to the solved O_2. Since the reaction rate constant k_{CR2} was not known its value had to be estimated via numerical simulations in an optimization framework. In addition, due to different values of diffusion coefficients of Sulfite ions (see Leaist [17]) $D_{SO_3{}^{2-},SO_4{}^{2-}/H_2O} = 1.0\ 10^{-9}\ m^2 s^{-1}$ with respect to the D_{O_2/H_2O} and the presence of catalyzer, the value of the effective diffusion coefficient D_{eff} had to be subjected to the optimization process, as well. Accordingly, a two parameter optimization has been performed where the optimization constraint was defined by the experimentally measured concentration snapshots at the given axial positions in the SFM for the three different flowrates, $(150 + 150), (75 + 75)$ and $(15 + 15)\ cm^3 h^{-1}$. Such variation of flowrates covers the interesting performance range of the SFM for the defined conditions, meaning that in case of the highest flowrate the convection dominates and the chemical reaction is limited by the diffusion. As a result the O_2 concentration is still measurable even at the outflow region. In the other limiting case, the convection is already suppressed enough to let the diffusion to supply the underlying chemical reaction with the reactant species. In this case the reaction runs through already at the inflow part of the SFM and no concentration of O_2 is measured at the outflow from the SFM. The optimal parameter combination providing the best fit with the such measured experimental results were found to be as $D_{\mathrm{eff}} = 1.0\ 10^{-9} m^2 s^{-1}$ and $k_{CR2} = 5.5\ 10^4\ L\ mol^{-1} s^{-1}$,

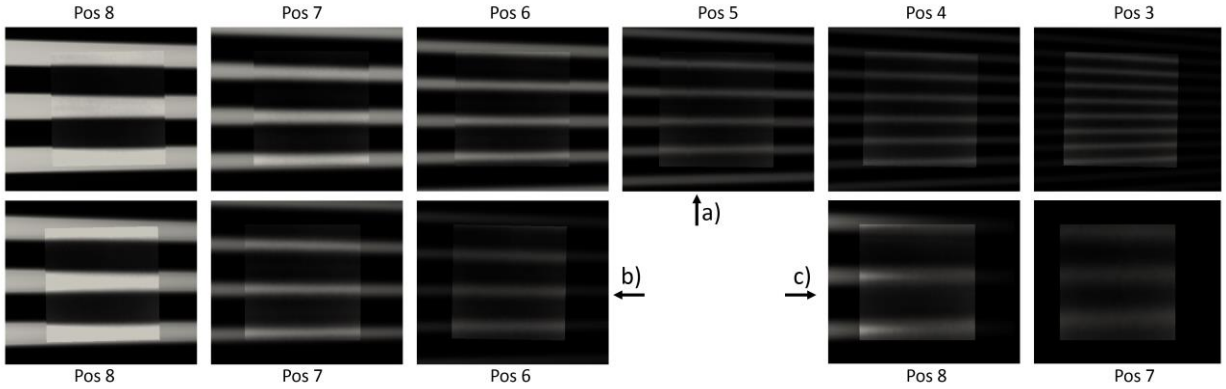

Fig 8 Simulation results obtained for the SuperFocus mixer for reactive mixing for flowrates a) 150, b) 75, and c) 15 $ml\ h^{-1}$ per each inlet stream. The greyscale corresponds to 0 to 12.0 $mg\ L^{-1}$.

for which the computationally obtained results are displayed in Fig. 8 with the experimentally observed concentration snapshots rendered into the computational results. From the sub-pictures referring to the different flowrates at different positions is visible that the agreement is pronounced

in the regions of high O_2 concentrations ($c_{O_2} > 2\ mg\ L^{-1}$) and the mismatch of results is to be seen in the regions below this threshold concentration. The regions characterized with a good agreement between experiment and simulation show a reasonable correlation between the decreasing widths of the O_2 concentration signal as well as between the reconstructions of the corresponding concentration shocks dictated by the diffusion. Considering the Sulfite to be in excess, an integral reaction rate constant can be estimated as $k^*_{\mathrm{CR2}} := k_{\mathrm{CR2}}\ c_{\mathrm{SO_3^{2-}}} = 176\ s^{-1}$. The corresponding computational cost for the simulations discretized by the same number of elements as in the physical mixing case are on the order of 3 times larger due to the simultaneous computation of three coupled transport equations.

Conclusions

In this work a numerical framework being suitable for simulations of micromixers has been developed, validated and used for simulations of reactive mixing in the SuperFocus Mixer. The main highlight of the numerical scheme, the algebraic grid deformation method, has proved to be an extremely important component of the complete numerical scheme especially in an interplay of other numerical ingredients described in the introduction of the work. The developed numerical scheme was shown to be suitable for reaction parameter determination in an optimization framework based on experimental observations associated with an oxidation reaction of Sodium Sulfite in an aqueous environment inside of the SuperFocus mixer.

Acknowledgement

The financial support of DFG (SPP 1740) is gratefully acknowledged (TU 102/53-1 / SCHL 617/12-1). The computations have been carried out on the LiDOng cluster at TU Dortmund. We would like to thank the LiDOng cluster team for their help and support.

Symbols Used

Notation

$\mathbf{x}$	$[m]$	position vector
$M(\mathbf{x})$	dimensionless	monitor function
$w(\mathbf{x})$	dimensionless	weight distribution
i, j	dimensionless	summation indices
e_{ij}	dimensionless	edges connecting the element vertices
ω	dimensionless	underrelaxation constant
N	dimensionless	total number
$d(\mathbf{x})$	$[m]$	the distance distribution
Re	dimensionless	Reynolds number
ϕ	$[mol\ L^{-1}]$	transported scalar quantity
c	$[mol\ L^{-1}]$	concentration
ρ	$[kg\ m^{-3}]$	density

μ	$[kg\ m^{-1}s^{-1}]$	kinematic viscosity
D	$[m^2s^{-1}]$	diffusion coefficient
k	$[L\ mol^{-1}s^{-1}]$	reaction rate constant

Subscripts

V	Vertices
CR	Chemical Reaction
EL	Elements
eff	effective
S	species

Superscripts

old	old value
new	new value

References

References

[1] K. Malecha, L. J. Golonka, J. Bałdyga, M. Jasińska, P. Sobieszuk, *Sens. & Actuators B: Chem.*, **2009**, 143, pp: 400-413.DOI: 10.1016/j.snb.2009.08.010.

[2] S. Cerbelli and M. Giona, *Chem. Eng. J.*, **2008**, *138*, pp. 523–537, DOI: 10.1016/j.cej.2007.07.067.

[3] S. Panic, S. Loebbecke, T. Tuercke, J. Antes, and D. Boskovic, *Chem. Eng. J.*, **2004**, *101*, pp. 409–419, DOI: 10.1016/j.cej.2003.10.026.

[4] V. Hessel, S. Hardt, H. Lowe, and F. Schönfeld, *AIChE J.*, **2003**, *49*. pp: 566–577, DOI: 10.1002/aic.690490304.

[5] P. Löb, K.S. Drese, V. Hessel, S. Hardt, Ch. Hofmann, H. Löwe, R. Schneck, F. Schönfeld and B. Werner, *Chem. Eng. Technol.*, **2004**, 27, pp:340–345, DOI: 10.1002/ceat.200401995.

[6] M. Hoffmann, M. Schlüter; N. Räbiger:, *Chem. Eng. Sci.*, **2006**, 61, pp. 2968-2976, DOI: 10.1016/j.ces.2005.11.029.

[7] S. Hardt and F. Schönfeld, *AIChE J.*, **2003**, *49*, pp. 578–584, DOI: 10.1002/aic.690490305.

[8] T. Glatzel, C. Litterst, C. Cupelli, T. Lindemann, C. Moosmann, R. Niekrawietz, W. Streule, R. Zengerle and P. Koltay, *Comput. Fluids*, **2008**, *37*, pp. 218–235, DOI: 10.1016/j.compfluid.2007.07.014.

[9] D. Bothe, A. Lojewski, H.-J.Warnecke, *AIChE J.*, **2009**, *56*, pp: 1406–1415, DOI: 10.1002/aic.12067.

[10] D. Kuzmin, R. Löhner, S.Turek, *Flux–Corrected Transport: Principles, Algorithms, and Applications*, Springer, **2005**.

[11] X.-X. Cai, B. Jiang and G. Liao, *Comput Math Appl*, **2004**, *48*, pp.:1077-1085, DOI: 10.1016/j.camwa.2004.10.006.

[12] M. Grajewski,; M. Köster,; S. Turek,, *SIAM J. Sci. Comput.*, **2009**, *31*, *DOI: 10.1137/050639387*.

[13] J. Paul, *PhD Thesis*, TU Dortmund, Dortmund, **2016**.

[14] T. Qiu, T. Lee, A. Mark, K. Morozov, R. Münster, O. Mierka, S. Turek, A. Leshansky, P. Fischer, *Nat. Commun.*, **2014**, *5*:5119, pp:1-8, DOI: 10.1038/ncomms6119.

[15] O. Mierka, S. Turek, *Numerical Simulation of Monodispersed Droplet Generation in Nozzles, Appeared in: Process-Spray: Functional Particles Produced in Spray Processes*, **2016**, Springer.
[16] H.L. Toor, S.H. Chiang, *AIChE J.*, **1959**, *5*, pp: 339–344, DOI: 10.1002/aic.690050317.
[17] D. G. Leaist, *Can. J. Chem.*, **1985**, *63*, pp: 2933–2940, DOI: 10.1139/v85-486.